The post-transcriptional regulatory system CSR controls the balance of metabolic pools in upper glycolysis of Escherichia coli

Manon Morin, Delphine Ropers, Fabien Letisse, Sandrine Laguerre, Jean-Charles Portais, Muriel Cocaign-Bousquet, Brice Enjalbert

Molecular Microbiology (2016) 00(00), 00–00

doi: 10.1111/mmi.13343
First published online 2016

The post-transcriptional regulatory system CSR controls the balance of metabolic pools in upper glycolysis of *Escherichia coli*

Manon Morin,[1,2,3,4] Delphine Ropers,[4]* Fabien Letisse,[1,2,3] Sandrine Laguerre,[1,2,3] Jean-Charles Portais,[1,2,3] Muriel Cocaign-Bousquet[1,2,3]*† and Brice Enjalbert[1,2,3]†

[1]*Université de Toulouse; INSA, UPS, INP, 135 Avenue de Rangueil, F-31077, Toulouse, France.*
[2]*INRA, UMR792 Ingénierie des Systèmes Biologiques et des Procédés, LISBP, F-31400, Toulouse, France.*
[3]*CNRS, UMR5504, F-31400, Toulouse, France.*
[4]*Inria Grenoble-Rhône-Alpes, 655 avenue de l'Europe, 38334, Montbonnot Cedex, France.*

Summary

Metabolic control in *Escherichia coli* is a complex process involving multilevel regulatory systems but the involvement of post-transcriptional regulation is uncertain. The post-transcriptional factor CsrA is stated as being the only regulator essential for the use of glycolytic substrates. A dozen enzymes in the central carbon metabolism (CCM) have been reported as potentially controlled by CsrA, but its impact on the CCM functioning has not been demonstrated. Here, a multiscale analysis was performed in a wild-type strain and its isogenic mutant attenuated for CsrA (including growth parameters, gene expression levels, metabolite pools, abundance of enzymes and fluxes). Data integration and regulation analysis showed a coordinated control of the expression of glycolytic enzymes. This also revealed the imbalance of metabolite pools in the *csrA* mutant upper glycolysis, before the phosphofructokinase PfkA step. This imbalance is associated with a glucose–phosphate stress. Restoring PfkA activity in the *csrA* mutant strain suppressed this stress and increased the mutant growth rate on glucose. Thus, the carbon storage regulator system is essential for the effective functioning of the upper glycolysis mainly through its control of PfkA. This work demonstrates the pivotal role of post-transcriptional regulation to shape the carbon metabolism.

Accepted 29 January, 2016. *For correspondences. M. Cocaign-Bousquet, E-mail: cocaign@insa-toulouse.fr; Tel. +33(0)561559465; Fax +33(0)561559400. D. Ropers, E-mail: delphine.ropers@inria.fr; Tel. +33(0)476615372; Fax +33(0)456527120. †These authors contributed equally to the work.

Introduction

The central carbon metabolism (CCM) supplies bio-precursors and energy in most living cells including the gram negative bacterium *Escherichia coli*. The interconnected pathways composing the CCM include glycolysis, gluconeogenesis, the tricarboxylic acid cycle (TCA cycle) and pentose phosphate pathways (PPP) (Holms, 1996). Carbon and energy fluxes in the CCM are highly regulated in a complex, multilevel network with many control loops (Heinemann and Sauer, 2010; Kotte *et al.*, 2010; Enjalbert *et al.*, 2011; Shimizu, 2014). In contrast to transcriptional and post-translational controls, the occurrence of post-transcriptional control (i.e., regulation of RNA stability and translation) remains poorly characterized in *E. coli*.

A post-transcriptional regulatory system considered to control various metabolic pathways is carbon storage regulator (CSR). The main component of the CSR system is the essential global regulator CsrA. This protein prevents the translation of target mRNA by binding near the ribosome binding site, thereby inhibiting translation and/or facilitating mRNA decay (Timmermans and Van Melderen, 2010; Seyll and Van Melderen, 2013; Duss *et al.*, 2014). CsrA can also mediate gene activation by stabilizing target transcripts, but the demonstration of such mechanisms is still rare in the literature (Wei *et al.*, 2001; Yakhnin *et al.*, 2013). The post-transcriptional regulatory system CSR has been directly demonstrated to be involved in the regulation of a wide range of physiological processes including biofilm formation, peptide uptake, motility, virulence and carbohydrate storage

Table 1. Macrophenotypic parameters for wild-type and *csrA51* strains during exponential growth. Parameter values (mean ± SD) are issued from three independent replicates as described in the *Experimental procedures*. Maximal growth rates, glucose-specific uptake rates, acetate and biomass yield, glycogen content and specific CO_2 production rates have been calculated during the exponential phase.

Medium	Parameter	WT	*csrA51*	Ratio
LB	Growth rate (h^{-1})	1.38 ± 0.07	1.26 ± 0.07	0.92[a]
LB glucose	Growth rate (h^{-1})	1.52 ± 0.04	0.96 ± 0.18	0.63[b]
M9 glucose	Growth rate (h^{-1})	0.57 ± 0.02	0.31 ± 0.02	0.54[b]
M9 glucose	Glucose consumption rate ($mmol_{GLC} \cdot h^{-1} \cdot gDW^{-1}$)	8.4 ± 0.1	5.3 ± 0.3	0.63[b]
M9 glucose	Acetate yield ($mmol_{ACE} \cdot mmol_{GLC}^{-1}$)	0.31 ± 0.02	0.02 ± 0.01	0.06[b]
M9 glucose	Glycogen content ($g_{glucose} \cdot gDW^{-1}$)	0.037 ± 0.003	0.252 ± 0.011	6.80[c]
M9 glucose	CO_2 production rate ($mmol_{CO2} \cdot h^{-1} \cdot gDW^{-1}$)	13.3 ± 0.50	8.9 ± 0.2	0.67[b]
M9 glucose	Biomass yield ($Cmol_{Biomass} \cdot Cmol_{GLC}^{-1}$)	0.46 ± 0.02	0.49 ± 0.02	1.05[a]

a. Similar values.
b. Lower values in the *csrA51* strain.
c. Higher values in the *csrA51* strain.

(Timmermans and Van Melderen, 2010; Romeo *et al.*, 2013).

The CSR system is also supposed to regulate CCM pathways. Several works (performed with different approaches, conditions and strains) have reported that CSR system is a potential regulator of a dozen targets in the CCM (positive effect for Pgi, PfkA, TpiA, Eno, PykF and Acs, and negative control for Pgm, GlgA, GlgB, GlgC, PfkB, Fbp, Pck and Pps) (Romeo *et al.*, 1993; Sabnis *et al.*, 1995; Yang *et al.*, 1996; Wei *et al.*, 2000; McKee *et al.*, 2012). Moreover, the CSR system is regarded as essential for growth on glycolytic media (Altier *et al.*, 2000; Timmermans and Van Melderen, 2009). This is a surprising property, given that other global or pleiotropic regulators such as RelA/SpoT, Crp-cAMP or RpoS are not essential (Adams and McLean, 1999; Nguyen *et al.*, 2011; Sabourin and Beckwith, 1975). The origins of this essentiality are unclear (Timmermans and Van Melderen, 2009; Revelles *et al.*, 2013). Taking as a whole, several clues supposed that the CCM is regulated by the CSR system but the physiological consequences of CSR-mediated regulations on the bacterial metabolism have not been characterized yet. It remains to be determined which of the multiple targets of CSR in the CCM are important for the cell physiology and if CSR could contribute in any extent to the coordination of these targets.

Here, we assessed the influence of CsrA on the CCM through a multilevel investigation (including growth parameters, gene expression levels, metabolite pools, enzyme activities and fluxes). These investigations were performed in a mutant strain with an attenuated CsrA protein and its isogenic wild type. The use of these datasets combined with modelling and experimental confirmations enabled us to demonstrate the crucial role of the CSR system in the control of the phosphofructokinase expression and its consequences on the upper part of the glycolysis. This work highlights for the first time the major role of post-transcriptional regulation in the correct tuning of the central carbon metabolism.

Results

The csrA51 *strain displayed a growth defect associated with a low glucose uptake rate*

To assess the influence of CsrA on the CCM, the behavior of strain *E. coli* MG1655 on glucose in various media was compared to its isogenic *csrA51* mutant strain. This strain is carrying an attenuated but viable variant of CsrA (deletion of the last 10 amino acids of the protein; see *Experimental procedures*). The construction and its resulting phenotypes on motility, biofilm production and glycogen content have been validated elsewhere (Esquerré *et al.*, submitted). As expected (Romeo *et al.*, 1993; Sabnis *et al.*, 1995), we confirmed that the mutation did not significantly affect the growth rate on rich LB medium in an Erlenmeyer flask (maximum growth rates $\mu = 1.26 \pm 0.07$ h^{-1} for the *csrA51* strain and 1.38 ± 0.07 h^{-1} for the wild type; Table 1). Due to the essentiality of *csrA* for growth on glucose, this carbon source is expected to negatively affect growth of the *csrA51* strain. Addition of glucose to the Lysogeny broth (LB) reduced the maximum growth rate of the *csrA51* strain to $\mu = 0.96 \pm 0.18$ h^{-1} while it increased the wild-type (WT) maximum growth rate to $\mu = 1.52 \pm 0.04$ h^{-1}. The negative influence of glucose on the mutant was also assessed by growing both strains on M9 minimal medium with glucose as the sole carbon source. The cultures were performed in well-controlled conditions in bioreactors (controlled oxygenation, temperature and pH; see *Experimental procedures*). In these conditions, the *csrA51* strain grew significantly more slowly than the WT strain with a maximum growth rate reduced to 54% of that of the WT strain (Table 1). Likewise, the specific consumption rate of glucose was 37% lower in the *csrA51* strain than in the

wild type. In both strains, acetate accumulated throughout the exponential phase but in the *csrA51* strain, acetate accumulation was reduced to 6% of that observed in the WT strain (Table 1). This confirms a previous result obtained in a strain with a reduced CsrA availability obtained by overexpressing *csrB*, a gene encoding a small RNA able to sequestrate *csrA* (McKee *et al.*, 2012). Aside from acetate, no fermentation products accumulated in the mutant, as demonstrated by total organic carbon assays (supporting information S1). As expected from the literature (Yang *et al.*, 1996), glycogen content is 6.8 times higher in the *csrA51* strain than in the wild type. CO_2 was also quantified in the gas phase where the production of CO_2 was demonstrated to be lower in the *csrA51* strain than in the WT (Table 1). Finally, the biomass yield from glucose consumption is similar in both the WT and *csrA51* strains. This suggests that the growth defect of the *csrA51* strain on glucose is not related to a decrease in the efficiency of biomass synthesis but rather to a reduction in the rate of glucose consumption.

CSR impact on CCM fluxes

The reduction of growth rate and glucose uptake rate in the *csrA51* strain should provoke a uniform decrease of the fluxes in the CCM. Beside this quantitative change, the *csrA51* mutation could also affect the flux partition through the local control of CSR-putative targets. Therefore, we determined the intracellular distribution of fluxes in the wild-type and *csrA51* strains by integrating uptake and secretion rates, as well as the biomass and glycogen production rates into a genome-scale reconstruction of the *E. coli* genome (Feist *et al.*, 2007). Since the glycogen content was found stable during the whole exponential phase of both strains (data not shown), the glycogen production rate was set up as a linear function of the growth rate. The biomass reaction was set to the measured growth rate. Constraints related to thermodynamics and to the composition of the growth medium were imposed (see *Experimental procedures* and supporting information S2 and S3). Metabolic flux analysis was performed, using as objective the minimization of the discrepancies between the predicted and measured fluxes (Antoniewicz, 2015). We further analysed the optimal solutions by flux variability analysis (Mahadevan and Schilling, 2003), to determine the minimum and maximum flux values satisfying the constraints and consistent with the measurements. This allowed restricting the possible values of intracellular fluxes to very tight intervals (Fig. 1 and Supporting Information S2 for details). In the *csrA51* strain, fluxes globally decreased in the CCM consistently with the decrease of glucose uptake rate. However, this decrease is not uniform with a higher diminution for the glycolytic flux compared to the TCA fluxes. Interestingly,

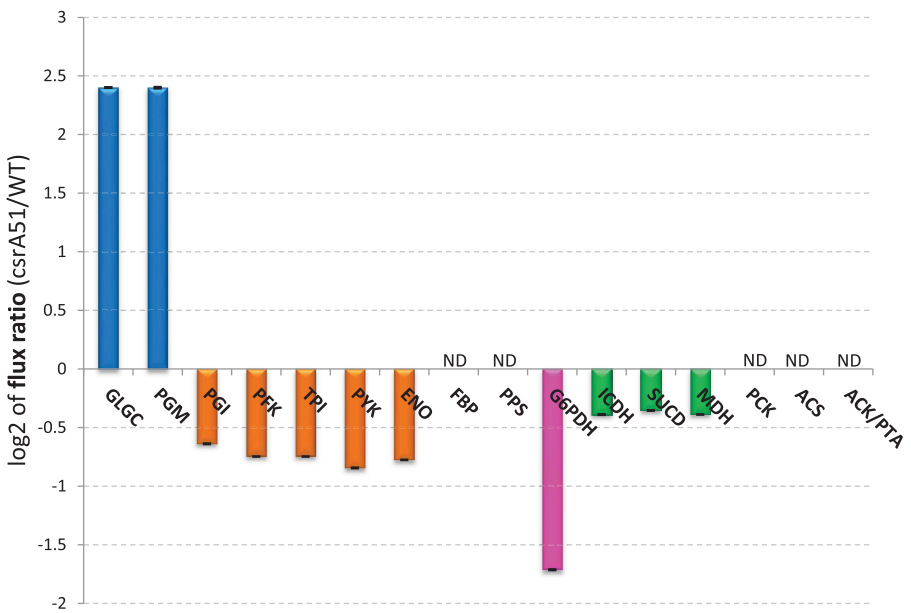

Fig. 1. Comparison of metabolic fluxes determined by FVA. A set of flux intervals was obtained for each strain from the integration of the three biological replicates (see *Experimental procedures* for details). The colour code matches the entity pathway (blue for the glycogen synthesis pathway, orange for the glycolysis pathway, pink for the pentose phosphate pathway, green for the TCA cycle. GLGC, glucose 1-phosphate adenyltransferase flux; PGM, phosphoglucomutase flux; PGI, phosphoglucose isomerase flux; PFK, phosphofructokinase flux; TPI, triose phosphate isomerase flux; PYK, pyruvate kinase flux; ENO, enolase flux; FBP, fructose biphosphatase flux; PPS, phosphoenolpyruvate flux; G6PDH, glucose 6-phosphate dehydrogenase flux; ICDH, isocitrate dehydrogenase flux; SUCD, 2-oxoglutarate decarboxylase flux; MDH, malate dehydrogenase flux; PCK, phosphoenolpyruvate carboxykinase flux; ACS, acetyl-coenzymeA synthetase flux; ACK/PTA, phosphate acetyltransferase and acetate kinase flux.

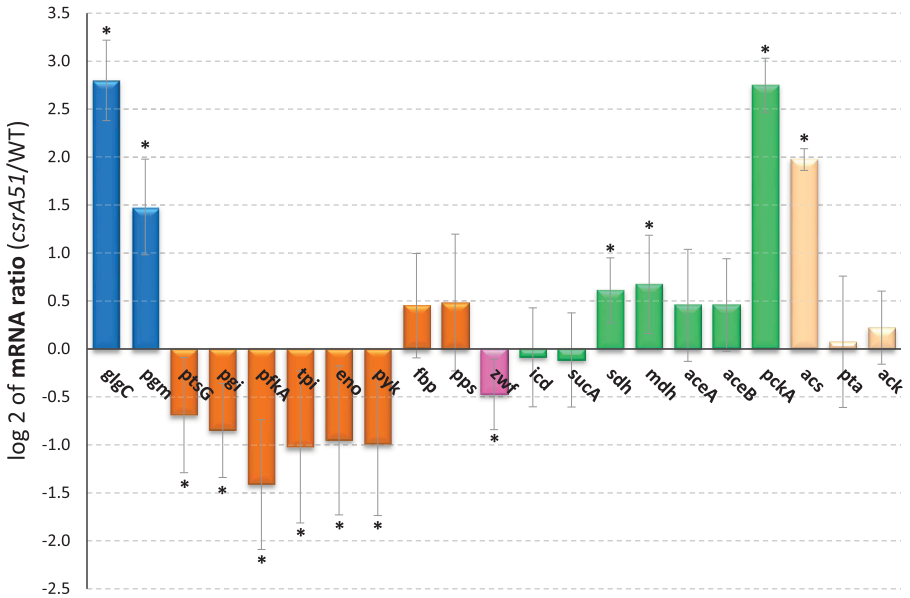

Fig. 2. Comparison of mRNA contents in the CCM between the wild type and the *csrA51* strains. mRNA data are issued from three independent replicates for the *csrA51* strain and its isogenic wild type (mean ± SD). The displayed values correspond to the log2 of the ratio of the *csrA51* strain to its isogenic wild type (with propagation of uncertainty). The asterisk represents significant ratio (*P* value <5% determined by *t*-test). The colour code matches the entity pathway (blue for the glycogen synthesis pathway, orange for the glycolysis pathway and gluconeogenesis pathways, pink for the pentose phosphate pathway, green for the TCA cycle and light brown for acetate metabolism pathway). glgC, glucose 1-phosphate adenyltransferase mRNA; pgm, phosphoglucomutase mRNA; ptsG, glucose PTS permease PtsG subunit mRNA; pgi, phosphoglucose isomerase mRNA; pfkA, phosphofructokinase A mRNA; tpi, triose phosphate isomerase mRNA; eno, enolase mRNA; pyk, pyruvate kinase mRNA; fbp, fructose biphosphatase mRNA; pps, phosphoenolpyruvate synthetase mRNA; zwf, glucose 6-phosphate dehydrogenase mRNA; icd, isocitrate dehydrogenase mRNA; sucA, 2-oxoglutarate decarboxylase mRNA; sdh, succinate dehydrogenase mRNA; mdh, malate dehydrogenase mRNA; aceA, isocitrate lyase mRNA; aceB, malate synthase mRNA; pck, phosphoenolpyruvate carboxykinase mRNA; acs, acetyl-coenzymeA synthetase mRNA; pta, phosphate acetyltransferase mRNA; ackA, acetate kinase mRNA.

the observed flux variations are constant inside both of these pathways. The strongest decrease was observed for the glucose-6-phosphate dehydrogenase flux (i.e., the first step towards the pentose phosphate pathway). Unlike in the CCM, higher fluxes were calculated in the glycogen synthesis pathway in the *csrA51* strain. We conclude that the phenotypic differences observed between both strains in Table 1 are associated with important flux reshaping.

CSR impact on CCM gene expression

The phenotypes and fluxes are deeply impacted in the *csrA51* strain. This is very likely to result from differential gene expression in the *csrA51* mutant. There is ample information about the effect of CSR on the CCM gene expression in the literature. However, this information is fractionated (and sometimes contradictory) as it is issued from works performed with a variety of measurement approaches, genetic backgrounds and growth conditions. We therefore re-investigated, for consistency, the impact of CSR on the gene expression levels during the exponential growth on M9 supplemented with glucose (Fig. 2). Higher expression of the *glgC* and *pgm* genes (both involved in glycogen biosynthesis) was found in the *csrA51* strain consistent with previous works (Romeo *et al*., 1993; Liu *et al*., 1995; Sabnis *et al*., 1995). All the glycolytic genes were significantly less expressed in the mutant (*ptsG*, *pgi*, *pfkA*, *tpi*, *eno* and *pyk*), while gluconeogenic genes (*fbp*, *pps*) presented nonsignificant variations. For the genes related to the TCA, strong up-regulation was detected for *pckA* while low or nonsignificant changes were observed for *icd*, *sucA*, *sdh*, *mdh*, *aceA* and *aceB*. In the acetate metabolic pathways, *acs* gene expression was up-regulated in the *csrA51* strain, while the expression of *pta* and *ackA* did not change significantly. Since these expression ratios have been obtained in the same experimental conditions, it is now possible to identify which genes are the most impacted by CsrA mutation. The highest impacts were observed for *glgC* and *pgm* (glycogen pathways), *pckA* (TCA pathways), *acs* (acetate metabolism) and *pfkA* (glycolysis pathway). To conclude, in the *csrA51* strain, the uniform down-regulation of glycolytic genes as well as the strong up-regulation of the genes involved in glycogen synthesis is consistent with the flux distribution described above.

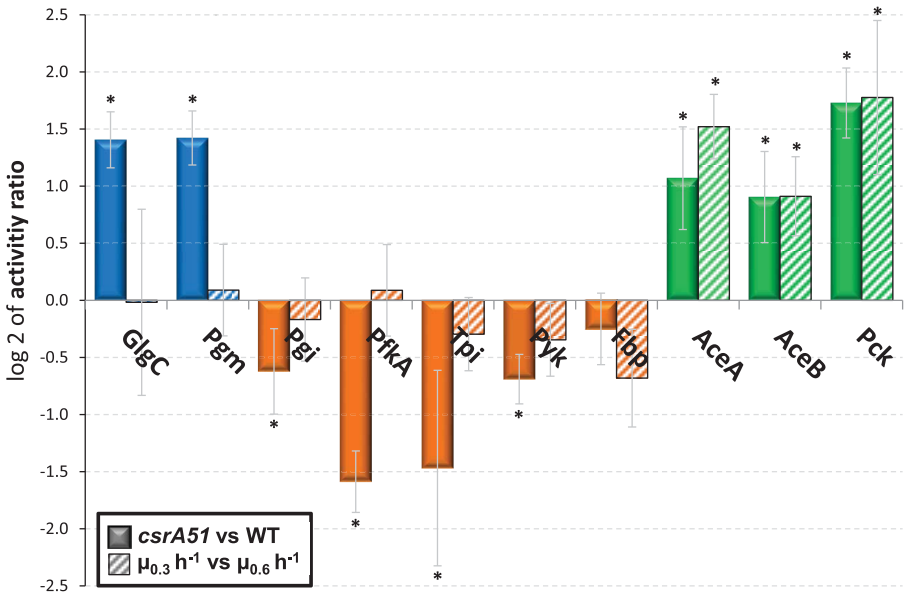

Fig. 3. Comparison of enzymatic levels in the CCM between the wild type and the *csrA51* strains or at different growth rates. Enzymatic levels are issued from three independent replicates for the *csrA51* strain and its isogenic wild type (mean ± SD). The displayed values correspond to the log2 of the ratio of the *csrA51* strain to its isogenic wild type (with propagation of uncertainty). Hatched columns represent log2 of ratio between enzymatic levels in the wild-type growing at $\mu = 0.3$ (chemostatic cultures) to the same strain at $\mu = 0.6$ (batch cultures). The asterisk represents significant ratio (*P* value <5% determined by *t*-test). The colour code matches the entity pathway (blue for the glycogen synthesis pathway, orange for the glycolysis pathway and gluconeogenesis pathways and green for the TCA cycle-related enzymes). GlgC, glucose 1-phosphate adenyltransferase; Pgm, phosphoglucomutase; Pgi, phosphoglucose isomerase; PfkA, phosphofructokinase A; Tpi, triose phosphate isomerase; Pyk, pyruvate kinase; Fbp, fructose biphosphatase; AceA, isocitrate lyase; AceB, malate synthase; Pck, phosphoenolpyruvate carboxykinase.

CSR impact on CCM enzymatic levels and metabolite pools

Besides its control on gene expression, CsrA is also known to modify translation level by interfering with the ribosome fixation. We therefore investigated if enzymatic levels follow differential gene expressions in the CCM (Fig. 3). As for their transcripts, the amount of glycogenic enzymes GlgC and Pgm was increased in the *csrA51* mutant while the glycolytic enzyme levels decreased. Abundances of the enzymes related to the TCA (AceA, AceB and PckA) were significantly enhanced in the CsrA mutant. Therefore, most of the observed enzyme level modifications were in good agreement with gene expression results.

We then investigated if the observed impacts on protein level could indirectly result from the growth rate reduction of the *csrA51* strain in regard to the wild-type strain. This was answered by using the data set from Esquerré *et al*. (2014) and by comparing enzymatic levels in the wild type in chemostatic growth at 0.3 h^{-1} (i.e., the *csrA51* growth rate) to the wild-type maximal growth rate on M9 glucose (0.6 h^{-1}). This revealed that decreasing the growth rate in the wild type increased levels of enzymes related to the TCA (AceA, AceB and Pck) like previously observed in the mutant. In contrast, glycogenic and glycolytic levels are mostly not affected by the growth rate reduction.

The huge impact of CsrA on the CCM is expected to modify the metabolite pools. We therefore investigated the concentrations of metabolites in both the *csrA51* mutant and the wild-type strains (Fig. 4). Glycogen content and the concentration of its precursor (ADP-glucose) were, respectively, 7 and 5 times higher in the *csrA51* strain. Likewise, metabolite pools from the upper glycolysis (G6P and F6P) were 2.5 times higher in the *csrA51* cells. Metabolite pools of the pentose phosphate pathway (6PG, S7P and R5P) increased from 1.5 to 7 times in the *csrA51* strain. In contrast, no significant difference was found in metabolite pools downstream of F6P in the glycolytic pathway (FBP, 2,3PG and PEP) or in the TCA, except for the fumarate pool, which was significantly reduced in the *csrA51* strain.

Again, we investigated if the differential metabolite concentrations could results from the reduced growth rate in the *csrA51* strain (Fig. 4). This revealed that the lower metabolite pools observed in the TCA cycle of the mutant could be explained by the growth reduction while the over-accumulation of metabolites in the upper glycolysis was more directly related to the mutation. These results strengthened that the core function of CSR in the CCM is the regulation of upper glycolysis activities to regulate the metabolic pools and glycogen production. This accumulation of metabolites was concentrated before the phosphofructokinase step, suggesting a key role of this particular enzyme.

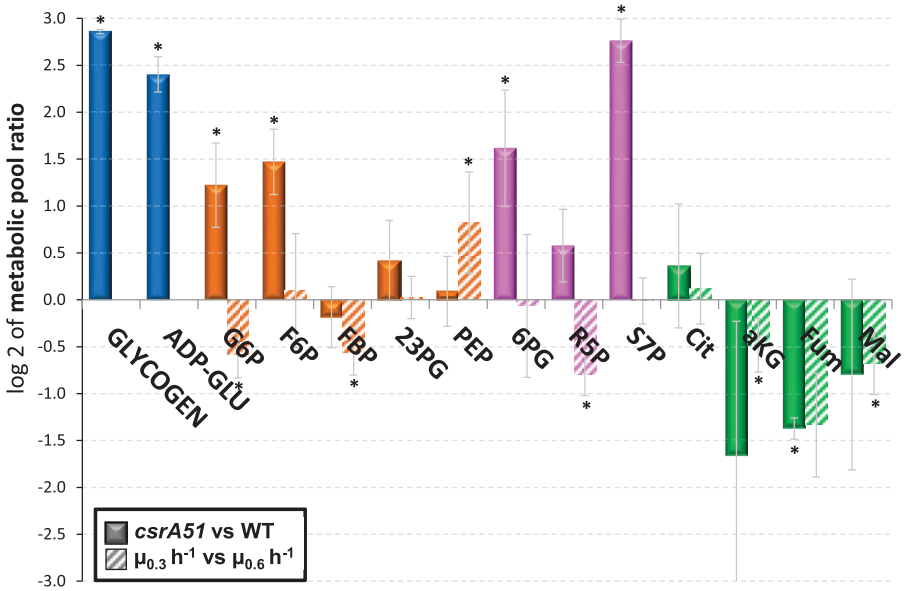

Fig. 4. Comparison of metabolite concentrations in the CCM between the wild-type and the *csrA51* strains or at different growth rates. Metabolic concentrations are issued from three independent replicates for the *csrA51* strain and its isogenic wild type (mean ± SD). The displayed values correspond to the log2 of the ratio of the *csrA51* strain to its isogenic wild type (with propagation of uncertainty). Hatched columns represent log2 of ratio between metabolite concentrations in the wild-type growing at $\mu = 0.3$ (chemostatic cultures) to the same strain at $\mu = 0.6$ (batch cultures). The asterisk represents significant ratio (*P* value <5% determined by *t*-test). The colour code matches the entity pathway (blue for the glycogen synthesis pathway, orange for the glycolysis pathway and gluconeogenesis pathways, pink for the pentose phosphate pathway and green for TCA cycle-related metabolites). G6P, glucose 6-phosphate; F6P, fructose 6-phosphate; FBP, fructose 1,6-biphosphate; 23PG, 3-phospho glycerate and 2-phospho glycerate; PEP, phosphoenolpyruvate; 6PG, 6-phospho glucono-1,5-lactone; R5P, ribose 5-phosphate and ribulose 5-phosphate; S7P, sedoheptulose 7-phosphate; cit, citrate; aKG, α-keto glutarate; Fum, fumarate; Mal, malate.

Glycolytic activities are mainly under hierarchical control

Major reorganization of the CCM has been described above in the *csrA51* mutant strain. CsrA is expected to regulate the levels of target enzymes and thus the corresponding fluxes. However, indirect control of fluxes by enzyme activities can also occur due to the important metabolome modifications observed in the *csrA51* strain. Hierarchical regulation analysis (ter Kuile and Westerhoff, 2001; van Eunen *et al.*, 2011) was therefore applied to the data to decipher the mode of flux control for glycolytic and glycogenic reactions (see *Experimental procedures* and supporting information S4 for details). Flux regulation was dissected into hierarchical regulation (ρ_h) and metabolic (ρ_m) coefficients, quantifying the contribution of changes in gene expression or metabolite pool to the flux change. The distributions of the resulting coefficients are displayed as boxplots in Fig. 5. Median values of ρ_h coefficients were close to 1 for most of glycolytic reactions (PYK, ENO, TPI and PGI) while higher values were obtained for glycogenic reactions (PGM and GLGC). All these ρ_h coefficients are positive, indicating that in the *csrA51* strain, changes in the catalyzing enzyme levels impose the flux changes. The metabolic regulations of these catalyzing enzymes, as indicated by the negative values of the ρ_m, are antagonistic to the flux changes and therefore secondary in the control of the reaction. The result was different for the phosphofructokinase (PFK). The values of the regulation coefficients ρ_h and ρ_m coefficients were similar and equal to 0.5, revealing a shared control of the flux. This indicates that 50% of the PFK flux variation in the *csrA51* strain could be attributed to metabolic changes within the cell and 50% to the modification of PfkA expression. Overall these results show that all the studied reactions are strongly affected at the level of their protein level by variations of the CsrA concentration. Only PFK appears to be controlled by CsrA through the combination of metabolic and hierarchical regulations.

Growth defect in the csrA51 *mutant is limited to substrates requiring phosphofructokinase activity and associated to glucose phosphate stress*

The *csrA51* strain presents a reduced glucose uptake rate (Table 1) combined to the accumulation of metabolites before the phosphofructokinase step whose activity is under dual genetic and metabolic control (Figs. 3 and 4). To link these observations, we grew the WT and *csrA51* strains on several glycolytic substrates entering the CCM

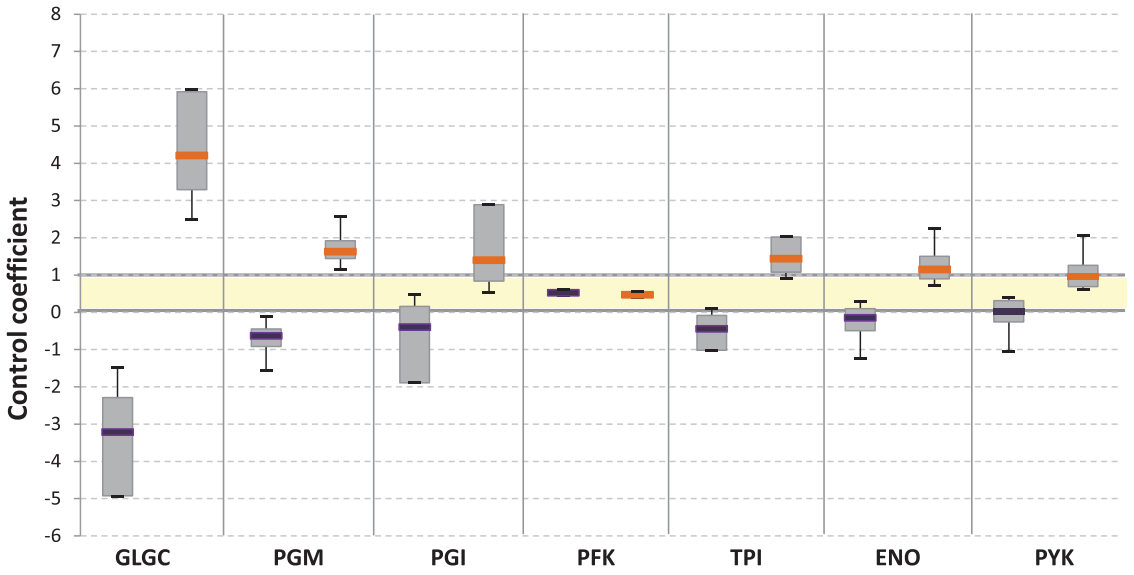

Fig. 5. Regulation of metabolic fluxes. Boxplots of the hierarchical and metabolic regulation coefficients calculated from the different replicates of the measured enzyme-specific activities and the flux bounds for each reaction (see *Experimental procedures* for details). Boxes represent the interquartile range (IQR) between the first and third quartiles. Whiskers denote the lowest and highest values within 1.5 × IQR from the first and third quartiles. Purple, median hierarchical coefficient; orange, median metabolic coefficient.

before (glucose and N-acetylglucosamine) or after (fructose and fucose) the PfkA-mediated metabolic step (metabolic pathways summarized in Fig. 6A). The *csrA51* strain displayed a growth defect on both N-acetylglucosamine and glucose, whereas no measurable difference was observed during growth on fucose or fructose on the WT (Fig. 6B). These results confirm that the growth defect of the *csrA51* strain originated in the early steps of glucose metabolisation and emphasize the PfkA regulation as a crucial control. A controversial report pinpointed the accumulation of glycogen as the cause of the growth defect of a *csrA* mutant on glucose due to hijacking of the carbon flux towards this reserve sugar (Timmermans and Van Melderen, 2009). This disagrees with our results, which establish the phosphofructokinase metabolic step as the pivot of the growth defect. To clarify this point, *csrA51* strains were grown on minimal media supplemented with either glucose, N-acetylglucosamine, fructose or fucose, and intracellular glycogen concentrations were quantified (Fig. 6B). Independently of the substrate, the *csrA51* cells accumulated much higher content of glycogen. Therefore, over-accumulation of glycogen in the *csrA51* strain is independent of the type of glycolytic substrate and hence independent of the growth defect. This result goes against the hypothesis of glycogen accumulation as the cause of the growth defect, as previously objected (Revelles *et al.*, 2013). We conclude that glycogen accumulation is more likely a side effect of CsrA attenuation.

G6P and/or F6P over-accumulations as observed in the *csrA51* mutant (Fig. 3) are known to trigger a feedback regulatory loop known as "glucose–phosphate stress" (Morita *et al.*, 2003; Vanderpool, 2007). The accumulation of these sugar phosphates indirectly induces the expression of the noncoding RNA SgrS (Vanderpool, 2007; Rice and Vanderpool, 2011). SgrS triggers the degradation of the *ptsG* mRNA, encoding an essential component of the glucose transport system (Fig. 6A). This results in a reduction of the glucose consumption rate, and hence, in a reduction of the sugar phosphate pools to counteract the stress. Since the pools of G6P and F6P were 2.5–3 times higher in the *csrA51* strain compared to WT and since the *ptsG* level was reduced (Figs. 2 and 4), we looked for molecular evidence of glucose–phosphate stress by investigating the level of expression of SgrS in both strains grown on glucose, N-acetylglucosamine, fructose and fucose. SgrS transcript levels were 5–7 times higher in the *csrA51* grown on glucose and N-acetylglucosamine respectively (Fig. 6B). Such induction was not found in the two strains grown on fructose or fucose. These results are evidence for the existence of a glucose phosphate stress coupled with a growth defect for the *csrA51* strain grown on substrates that require phosphofructokinase activity. In conclusion, *csrA51* growth defect is not associated to a glycogen accumulation but to a glucose–phosphate stress when the mutant is grown on substrate entering the glycolytic pathway above the phosphofructokinase step.

Overexpression of PfkA suppresses the hexose phosphate stress and partially restores the growth rate of the csrA51 *mutant*

A deletion of *pfkA* has been reported to present a strong growth defect on glucose medium with a growth rate

COLOR

6A.

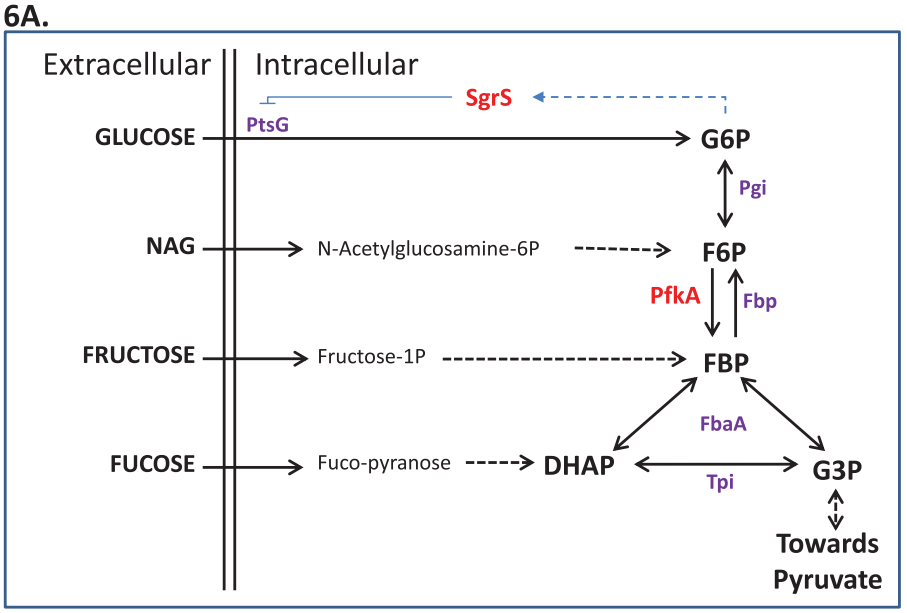

6B.

Substrate	μ WT h^{-1}	μ *csrA51* h^{-1}	μ Ratio	Glycogen WT $g_{gluc}.gDW^{-1}$	Glycogen *csrA51* $g_{gluc}.gDW^{-1}$	Glycogen Ratio	sgrS WT AU	sgrS *csrA51* AU	sgrS Ratio
Glucose	0.57 ±0.01	0.32 ±0.01	**0.56** ±0.02	0.037 ±0.003	0.252 ±0.011	**6.80** ±0.64	28 ±7.3	136.9 ±18.7	**4.9** ±1.4
NAG	0.53 ±0.02	0.34 ±0.01	**0.64** ±0.03	0.022 ±0.012	0.318 ±0.033	**14.20** ±7.32	27.3 ±2.7	192.4 ±23	**7** ±1.1
Fructose	0.38 ±0.01	0.37 ±0.02	0.98 ±0.06	0.013 ±0.001	0.217 ±0.065	**16.31** ±5.08	17.3 ±5.1	19.5 ±0.02	1.1 ±0.4
Fucose	0.43 ±0.02	0.43 ±0.01	0.99 ±0.05	0.017 ±0.004	0.287 ±0.065	**16.89** ±5.77	18.3 ±1.5	20 ±13.5	1.1 ±0.7

Fig. 6. Properties of *E. coli* grown on a variety of glycolytic substrates.
A. Simplified representation of the metabolic pathways and point of entry in the CCM for four glycolytic substrates.
B. Growth rates, glycogen contents and SgrS level of expression for the wild-type and the *csrA51* strains on a variety of glycolytic substrates. Each growth rate, glycogen content and SgrS levels is issued from the mean ± SD of three independent biological replicates. The ratio *r* = *csrA51*/WT is given for each substrate.

close to 0.1 h^{-1} (Fischer and Sauer, 2003; Nakahigashi *et al.*, 2009). We therefore hypothesized that the limited PfkA activity inherent to the *csrA51* strain could be sufficient to explain the growth defect directly by blocking the glycolytic pathway, or indirectly through the feedback loop of the glucose phosphate stress. We assessed this by overexpressing the *pfkA* gene in the WT and *csrA51* strains and growing them on M9 glucose (Fig. 7). Measurements of *pfkA* mRNA levels and of PFK enzymatic activities showed that the overexpression enabled *pfkA* expression and phosphofructokinase activity to be restored in the *csrA51* strain (Fig. 7A and B). We then investigated the effect of *pfkA* overexpression on G6P metabolic pool and on SgrS accumulation. While *csrA51* increased the G6P pool, the overexpression of *pfk*A abolished the phenomenon (Fig. 7C). As expected from the moderate G6P pool, the SgrS induction in the *csrA51* mutant is prevented by pfkA overexpression (Fig. 7D). The overexpression did not prevent glycogen accumulation (Fig. 7E). Finally, overexpression of *pfkA* moderately but significantly increased the growth rate in the *csrA51* strain (Fig. 7F). Taking as a whole, these results comfort PfkA as a most important target of the CSR system in the central carbon metabolism.

Discussion

The present work reveals the major role of post-transcriptional regulation in the control of the central carbon metabolism of *E. coli*. The multilevel analysis and data integration demonstrated the strong control of the CSR post-transcriptional regulatory system in the upper part of the glycolysis. Attenuation of CsrA activity results in a decrease in most glycolytic activities, especially the phosphofructokinase. This was shown to provoke an accumulation of metabolites in the top of glycolysis before the phosphofructokinase step and hence a glucose–phosphate stress controlling negatively the sugar uptake. Consequences of this cascade of regulations

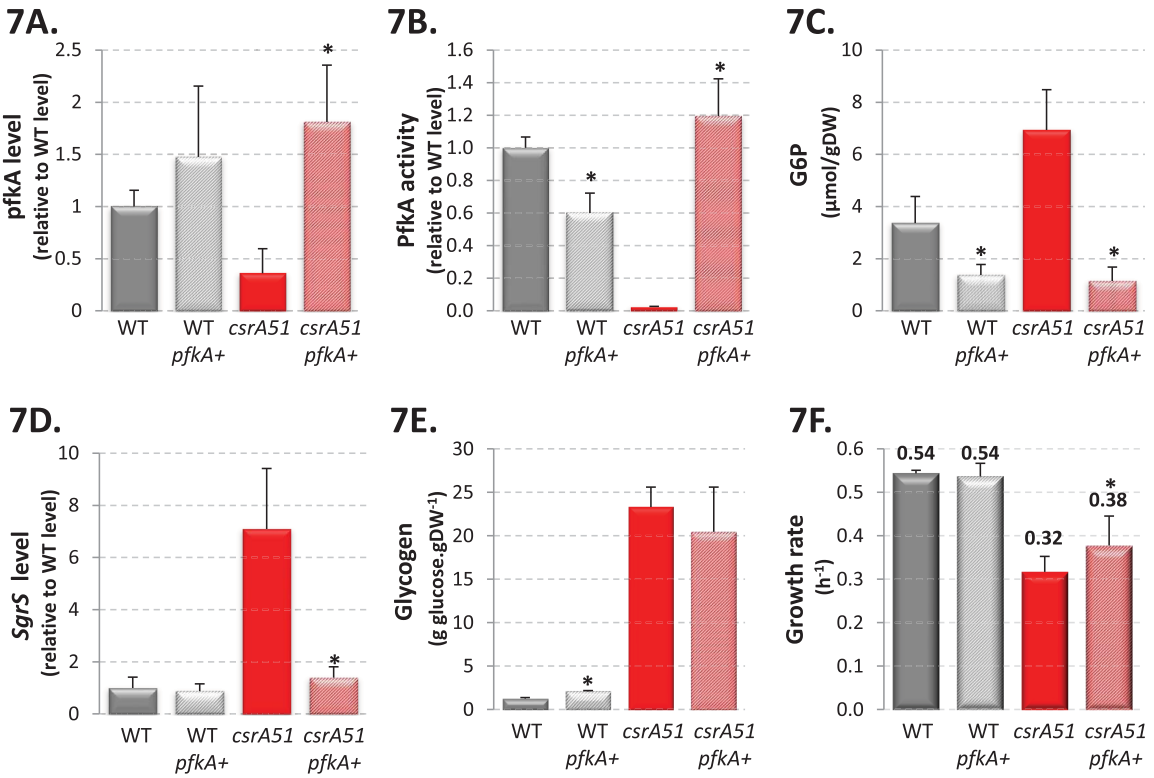

Fig. 7. Overproduction of *pfkA* in the wild-type and *csrA51* strains. Wild-type or *csrA51* strains were transformed by the empty vector or the vector carrying the *pfkA* gene ("*pfkA*+").
A. *pfkA* mRNA levels in the four strains.
B. PfkA-specific activities in the four strains.
C. G6P concentration in the four strains.
D. SgrS ncRNA levels in the four strains.
E. Glycogen content in the four strains.
F. Growth rates of the four strains. Each value is issued from the mean ± SD of three independent biological replicates. The asterisk represents significant differences between the strain overexpressing *pfkA* and its control (*P* value <°5% determined by *t*-test).

are dramatic for the cell growth rate, and we propose this explains the essentiality of the CSR system on glucose.

Influence of the CSR system over the CCM has already been reported in the literature. However, the information was limited to one level of observation [for example, activities in Sabnis *et al*. (1995), proteomic in McKee *et al*. (2012) and fluxes in Revelles *et al*. (2013)]. Besides, the medium and strains were very different from one paper to another, making comparison very awkward [Kornberg rich medium and model strain BW3414 in Sabnis *et al*. (1995), MOPS-based medium and industrial strain BLR in McKee *et al*. (2012), M9 medium and strain Nissle 1917 belonging to the phylogenetic group B2 in Revelles *et al*. (2013)]. The strength of the present work is to provide the first coherent investigation of the CSR influence on the CCM through the measurement of growth properties, enzyme activities, metabolite pools and fluxes of the model bacterium *E. coli* MG1655. It confirms that the CSR system controls several pathways of the CCM (glycogenesis, glycolysis, gluconeogenesis, TCA cycle and acetate metabolism). The multilevel investigation also allowed demonstrating that the control is largely exerted at the gene expression level with repercussions on enzyme activities and fluxes distribution. Some previously identified targets like Fbp or Pck were shown to result from the growth rate modification triggered by the CsrA mutation during glucose consumption. This permitted to refine the list of CSR targets in the CCM to the upper glycolysis and glycogenesis and this finding was corroborated by the accumulation of metabolites in this pathway for the *csrA51* mutant. Very interestingly, all the five glycolytic steps studied in this work (PGI, PFK, TPI, PYK and ENO) displayed a coherent decrease in their gene expressions, of enzyme abundances, and flux ratios in the *csrA51* strain. This was corroborated by the predominant hierarchical control of their glycolytic fluxes. Thus, these results strongly suggest that glycolytic enzymes are under direct and coordinated regulation by CsrA.

CsrA has been reported to be essential for *E. coli* growth on glycolytic substrates because it over-

accumulates glycogen (Timmermans and Van Melderen, 2009). We show here that attenuation of the essential CsrA post-transcriptional regulator creates a growth defect in presence of glucose in rich or minimal medium. The accumulation of glycogen was observed in the *csrA51* strain, independently of the growth rate default. This suggests that glycogen accumulation is not the actual cause of the CsrA essentiality. The growth defect was not observed with all glycolytic substrates (i.e., not on fructose or fucose) and was related to the upper part of glycolysis. Using systematic analysis of CCM components in the wild-type and *csrA51* strains, we discovered that most of the molecular discrepancies between the two strains are indeed located in the close vicinity of the point of glucose entry into the central carbon metabolism. The most down-regulated enzyme of the glycolytic pathway was PfkA. Since substrates entering the CCM after this metabolic step are not associated with a *csrA51* growth defect, we hypothesized that down-regulation of PfkA creates an engorgement of the metabolic fluxes in the first glycolytic reaction that could lead to the growth deficiency. This hypothesis was supported by the observed higher pools of F6P and S7P [i.e., the two PfkA substrates (Nakahigashi *et al*., 2009)] and more largely by the accumulation of metabolites in the top of glycolysis before the PfkA step. Restoring a wild-type level of PfkA in the *csrA51* mutant prevent these metabolite accumulation and partially restore the growth rate. From all these elements, we conclude that PfkA plays a major role in the *csrA51* phenotypes. However, all the consequences of the *csrA51* mutation on the CCM cannot be mediated through PfkA down regulation only. First, the *pfkA* deletion does not entirely prevent growth on glucose minimal medium as observed in a strain in which *csrA* is deleted (Nakahigashi *et al*., 2009; Timmermans and Van Melderen, 2010). Second, restoring the WT level of PfkA expression did not entirely restore a WT growth rate in the *csrA51* strain (this work). Glycolytic flux control is known to be shared among its enzymes in microorganisms (Smallbone *et al*., 2013). This might explain why the influence of the CSR system is so dramatic since it controls the expression of most of the glycolytic enzymes conjointly, among which PFK appears to be the most crucial metabolic step.

An important metabolic consequence of the reduced glycolytic fluxes is the accumulation of sugar phosphates G6P and F6P. F6P and S7P were reported to accumulate in the *csrA51* mutant of the Nissle 1917 background, but not G6P. We demonstrated here that the accumulation of hexose phosphate triggers glucose phosphate stress as a feedback control in the *csrA51* strain through the expression of its characteristic marker SgrS (Vanderpool, 2007; Rice and Vanderpool, 2011). SgrS is known to reduce glucose transport by facilitating the degradation of the *ptsG* messenger. This was confirmed by our multilevel analyses, which revealed reduced *ptsG* expression in the *csrA51* strain. Overexpression of *pfkA* in the *csrA51* strain suppressed the glucose–phosphate stress and partially restored the growth. Thus, CsrA attenuation results in a subefficient glycolysis unable to absorb the G6P pool which trigger SgrS and reduced glucose entrance in the cell. On the basis of our results, we proposed that *csrA* essentiality is due to its essential role to promote glycolysis. This suggests that the primary function of the CSR system in the CCM is to adjust the glycolytic activity to the carbon availability and cellular requirement. CSR was previously proposed to fine tune the stringent response (Edwards *et al*., 2011), which is also related to the growth rate response. This reinforces that one function of the CSR system is to coordinate the fine tuning of the glycolytic activities and the growth rate.

Post-transcriptional regulation of central carbon metabolism has been almost ignored so far, but it now appears to play a crucial role in its correct tuning. One drawback in biotechnology approaches is the robustness of the CCM system (Sauer *et al*., 1999). It was recently shown that *csrB* overexpression is of interest for biotechnologies since it produces low levels of fermentation products (McKee *et al*., 2012). Here, we demonstrate the high potential of CSR mutants in biotechnologies since they allow reshaping of the CCM metabolic pools and fluxes. These new organizations offer many opportunities such as exploiting the larger pools of sugar phosphates to ensure the production of high added value compounds.

Experimental procedures

Strains

The strains used in this study were the wild-type strains *E. coli* K12-MG1655 and the previously constructed and validated *csrA51* strain corresponding to a partial deletion of the 10 last amino acids of the CsrA protein by using λ red system recombination (Esquerré *et al*., submitted). *pfkA* overexpression in the wild type or the *csrA51* background was achieved by cloning a 1963 pb fragment including *pfkA* and its promoter into the Kpn1-HindIII sites of a pUC19 plasmid. The fragment was amplified from the MG1655 genome (5′Primer: ATTGAGGTACCGATGAGGAACGGAAGGAAGAAATTATTG and 3′Primer: TAACTAAGCTTG AATCACCACGTTATCACCAGTTT).

Media and growth conditions

Bioreactor cultures were performed in 500 ml of M9 medium complemented with 2.7 g · l^{-1} of *D*-glucose. The

cultures were inoculated at an optical density of 0.2 after overnight preculture of the wild-type strain and a 48 h preculture of the *csrA51* strain. At least three independent replicates were made for each strain in the same conditions (stirring at 800 r.p.m., pH 7, 37°C and air flow at 0.2 l · s^{-1}). These parameters were set and monitored using a Multifors bioreactor system (Infors, Switzerland). The percentages of CO_2 and O_2 in the gas output were determined using a Dycor ProLine Process Mass Spectrometer (Ametek, DE, USA). During the cultures, OD and extracellular metabolites were measured every 30 min. Several samples were taken for enzymatic assays, intracellular metabolites analysis and qPCR experimentations during the midexponential phase of the culture (OD = 1.5) for each biological replicate. Growth in chemostat was performed in M9 glucose using a 0.5 l Sartorius bioreactor controlled by a Biostat Qplus device as described in Esquerre *et al.* (2014). Cultures in LB or on the range of substrates as well as for *pfkA* overexpression were performed in a baffled shake flask at 37°C in 50 ml of M9 glucose complemented with either 2.7 g · l^{-1} *D*-glucose, 2.7 g · l^{-1} *D*-fructose, 2.45 g · l^{-1} *L*-fucose, or 2.5 g · l^{-1} N-acetyl-(*D*)-glucosamine.

Calculation of fermentation parameters

For all the cultures, different growth parameters were calculated during the exponential phase of growths. All these parameters remained constant during this growth phase. The maximum growth rate in h^{-1} was calculated by determining the mean of all the instant growth rates acquired during the exponential phase using the following equation where *X* is the biomass concentration in gDW · l^{-1}:

$$\mu = \frac{dX}{dt} * \frac{1}{X} \quad (1)$$

The maximum glucose uptake rate ($mmol_{GLU}$ · h^{-1} · gDW^{-1}) was calculated by determining the mean of all the instant glucose uptake rates acquired during the exponential phase using the following equation:

$$qS_{GLU} = \frac{dGLU}{dt} * \frac{1}{X}. \quad (2)$$

Acetate yield was calculated by determining the mean of all the instant acetate yields acquired during the exponential phase using the following equation:

$$Y_{ACE/GLU} = \left| \frac{\Delta ACE}{\Delta GLU} \right|. \quad (3)$$

CO_2 production rate ($mmol_{CO2}$ · h^{-1} · gDW^{-1}) was calculated by determining the mean of all the instant CO_2 production rates acquired during the exponential phase using the following equations set:

$$qP_{CO_2} = \frac{1}{X} * (CO_{2OUT} - CO_{2IN}), \quad (4)$$

$$CO_{2OUT}\ (g_{CO_2} \cdot h^{-1} \cdot l^{-1}) = \frac{Q_{OUT} * Fm_{CO_2} * M_{CO_2}}{Vm_{CO_2} * Vf}, \quad (5)$$

$$CO_{2IN}\ (g_{CO_2} \cdot h^{-1} \cdot l^{-1}) = \frac{Q_{IN} * Fm_{CO_2} * M_{CO_2}}{Vm_{CO_2} * Vf}. \quad (6)$$

Q_{OUT} is the air outflows (g_{air} · h^{-1}), Q_{IN} is the air inflows (g_{air} · h^{-1}), Fm_{CO2} is the molar fraction of CO_2 in the air, M_{CO2} corresponds to the CO_2 molar mass, Vm_{CO_2} is the CO_2 molar volume and *Vf* the medium volume.

Enzymatic assays

The equivalent of 40 mg of dried cells was sampled during bioreactor cultures to perform enzymatic assays. The cells were pelleted (10 min at 6000 r.p.m. at 4°C) before being washed twice with 0.2% KCl (v/v) and resuspended in 2 ml of a Tris–carballylic acid breaking buffer (Tris–tricarballylate pH 7.8, 2.7 M glycerol, 50 mM $MgCl_2$, 300 mM DTT). The cells were then mechanically broken by six beating cycles of 30 s each separated by 1 min on ice using a Mini-Beadbeater2 (Biospec Products, Bartlesville, OK, USA) and Sigma glass beads (0.6 g of glass beads for 1 ml of cells). The cell extract was isolated after centrifugation (13,200 r.p.m. at 4°C for 15 min) and used in the following hours for enzymatic assays. Eleven enzymatic activities were obtained by measuring the changes in NADH or NADPH concentration at 340 nm using the SPECTRAmax PLUS^{384} microplate reader (Molecular Devices, Sunnyvale, CA, USA). All the reagents used were purchased from Sigma–Aldrich (USA). The optical density was measured at 7 s intervals for 10 min with a 3 s shaking phase between readings. The assays were performed in a total volume of 200 µl (including 10, 20 or 40 µl of extract) at 37°C, and the reactions were started by adding the substrate. Enzyme activities were determined from the linear part of the reaction. The total protein concentration in each extract was quantified by Bradford assay (Bio-Rad Protein assay, Bio-Rad, Germany) at 595 nm to obtain specific activities (µmol · g_{prot}^{-1} · h^{-1}) (Bradford, 1976). Phosphoglucoisomerase (Pgi) was assayed in the nonphysiologic direction using Tris–HCl buffer (0.1 M, pH 7.8), $MgCl_2$ (5 mM), NADP (5 mM), glucose 6-phosphate-1-dehydrogenase (0.2 U) and fructose 6-phosphate (10 mM). Phosphofructokinase (Pfk), triosephosphate isomerase (Tpi) and enolase (Eno) assays were performed as described in Even *et al.* (2001). Pyruvate kinase (Pyk) was measured using a modified method derived from Even *et al.* (2001): fructose 1,6-diphosphate (3 mM) was added to the assay and GDP (30 mM) was replaced by ADP (30 mM). Acetyl-coenzyme A synthetase (Acs) was assayed as developed by Castano-Cerezo *et al.* (2009); the isocitrate lyase (AceA) assay was performed as described in Van der Werf *et al.* (1997). We also followed this author's protocol for the phosphoenolpyruvate carboxykinase assay (PckA) but in a Tris–HCl buffer (0.1 M, pH 7.8). The fructose bisphosphatase (Fbp) assay was adapted from Peng and Shimizu (2003) by replacing the buffer with a Tris–HCl buffer (50 mM, pH 7.8). The phosphoglucomutase (Pgm) assay was that of (Joshi, 1982) using 40 mM of the same Tris–HCl buffer. Glucose 1-phosphate adenyltransferase (GlgC) was measured using phosphate buffer (100 mM, pH

Table 2. RT-PCR primers used in this work.

Name	Sequence (5′–3′)	Name	Sequence (5′–3′)
Q-aceA-3′	AACCAGCAGGGTTGGAACG	Q-aceA-5′	ACATGGGCGGCAAAGTTTTA
Q-aceB-3′	TCAGGCCATAAATCGGCACA	Q-aceB-5′	GGTGAACGCACCGAAGAAGG
Q-ack-3′	TCTTCCACCTGCACGACACC	Q-ack-5′	TCGCTGGTCACTTCGGTCAG
Q-acs-3′	GGATCTTCGGCGTTCATCTC	Q-acs-5′	GGGAAAATTGACTGGCAGGA
Q-eno-3′	GGGTGGTTTCGTCGGTATGG	Q-eno-5′	CCAGGAAACGGGATTTGTCG
Q-fbp-3′	GTAGAGATAAATACCGCCTTTCAGCA	Q-fbp-5′	ATAAATCCACCAACCGCCCTTA
Q-glgC-3′	AGATCACCGAAGCCGGTCTG	Q-glgC-5′	GTACCCACATCGCGCCAGTA
Q-icd-3′	TTCGTCACCGATGTTTGCAC	Q-icd-5′	CGCCTGTATGAACCTGAACG
Q-idnT-3′	AACACCGTGCGCCTCTTCTT	Q-idnT-5′	TTACGTCGGCCCAGTGTGAA
Q-ihfB-3′	CAAAGAGAAACTGCCGAAACC	Q-ihfB-5′	GCCAAGACGGTTGAAGATGC
Q-mdh-3′	TGGCCCATAGACAGGGTTGC	Q-mdh-5′	CCGAGCAGGAAGTGGCTGAT
Q-pck-3′	GTGTCTACGCCCGGCAGTTC	Q-pck-5′	GACGCCATCCTCAACGGTTC
Q-pfkA-3′	CACCCATGTAGGAACCGTCA	Q-pfkA-5′	AATTCCGCGACGAGAACATC
Q-pgi-3′	AGATCCGGCAACGCTTGACT	Q-pgi-5′	CCCAGGCTGAACGGAGTGAT
Q-pgm-3′	ATAACCCGCCGGAAGATGGT	Q-pgm-5′	AGTGCGTTGGCCCTGTCTTC
Q-pps-3′	CTGGCTCGTAACGCTCACCA	Q-pps-5′	GTGCCGCGTTTTATCCGAAG
Q-pta-3′	ACCGTGTTGCAGCGTCTCAG	Q-pta-5′	GCAGTTCGACCAGACGACCA
Q-ptsG-3′	GGAATGTCGCCGTGGAAAAC	Q-ptsG-5′	CCGTTTGGTCTGCACCACAT
Q-pykF-3′	GCAACCATGATGCCGTCAGA	Q-pykF-5′	CGGCGAAAACATCCACATCA
Q-sdhD-3′	ACACACCCCACACCACAACG	Q-sdhD-5′	CGTTAAACCGCTGGCTTTGC
Q-sgrS-3′	TCACACATGATGCAGGCAAGTCA	Q-sgrR-5′	GGTTGCGTTGGTTAAGCGTCCC
Q-sucA-3′	GGTGTCAGGGTCGGAGATCG	Q-sucA-5′	ACGGGAGTCAAACCGGATCA
Q-tpi-3′	CATCGGCGCACAGTACATCA	Q-tpi-5′	GCTCTTTCAGCACCGCGAAT
Q-zwf-3′	GCCCTTCGATCCCCACTTCT	Q-zwf-5′	GGCGCTGCGTTTTGCTAACT

7.8), $MgSO_4$ (5 mM), NADP (0.5 mM), fructose 1,6-diphosphate (10 mM), glucose 6-phosphate1-dehydrogenase (0.2 U), phosphoglucomutase (1 U) and ADP-glucose (8 mM). Malate synthase (AceB) was assayed in Tris–HCl buffer (0.1 M, pH 7.8), $MgSO_4$ (5 mM), acetyl-CoA (4 mM), NAD (3 mM), malate dehydrogenase (4 U) and glyoxylate (4 mM).

Extracellular and intracellular metabolites

The extracellular metabolites were identified and quantified using H+ HPLC (Agilent Technologies 1200 Series HPLC and Aminex HPX-87H column for acid and sugar separation). The analysis was carried out at 48°C using H_2SO_4 5 mM as eluent.

Intracellular metabolites were sampled at the mid-exponential phase using the differential method of Taymaz-Nikerel *et al.* (2009): 120 μl of broth or filtered culture (Sartolon polyamide 0.2 μm, Sartorius, Goettingen, Germany) were mixed with 1.25 ml of a quenching solution composed of 40% methanol, 40% acetonitrile and 20% water in a hemolysis tube. The tubes were stored at −20°C until analysis. A total of 120 μl of a fully ^{13}C-labeled cell extract were added to each tube as internal standard before the extracts were evaporated for 5 h in a SC110A SpeedVac Plus (ThermoFischer, MA, USA). The pellet was then resuspended in 120 μl of ultrapure water. Intracellular metabolites were quantified by high-performance anion exchange chromatography (Dionex ICS 2000 system, CA, USA) coupled to a triple quadrupole QTrap 4000 mass spectrometer (AB Sciex, CA, USA). The signals were processed and quantified using Analyst software (Analyst Software, AB SCIEX, USA).

RT-PCR analysis

Gene expression levels were analysed using Q-PCR in micro-Fluidigm or classical RT-PCR. At the mid-exponential phase, the equivalent of 5 mg of cells (dry weight) was harvested and directly flash-frozen in liquid nitrogen. RNA extraction was performed according to the TRIZOL method for *E. coli* described in Esquerré *et al.* (2014) and the concentration of RNA was determined using a Nanodrop® spectrophotometer. After a quality control by capillary electrophoresis (Bioanalyzer from Agilent, Santa Clara, CA, USA), the samples were subjected to reverse transcription using the Superscript II Reverse transcriptase (Life Technology). The Q-PCR EvaGreen experiment (Mao *et al.*, 2007) was performed on a Biomark 96.96 dynamic array (Fluidigm, San Francisco, CA, USA). Ninety samples were tested against 33 pairs of designed primers (Table 2) in technical triplicate. An internal control of human DNA was used to check the efficiency and quality of the run. Briefly, the experiment was carried out in three steps. First, in each cDNA sample, targeted cDNA was amplified using the pool of primers and TaqMan® PreAmp Master Mix (Fluidigm, San Francisco, CA, USA) with the following program: (i) 10 min at 95°C, (ii) 14 cycles of 15 s at 95°C and 4 min at 60°C. The samples were then treated with exonuclease ExoI (for 30 min at 37°C for digestion and for 15 min at 80°C for inactivation). Finally, the samples were added to a premix (2X TaqMan Gene Expression Master Mix, 20X DNA Binding Dye Sample Loading Reagent, 20X EvaGreen® and TE buffer) before being loaded into the macroarray. The sets of primers were loaded into the macroarray at a concentration of 20 μM. Control *idnT* values were used to normalize the data.

A classic RT-PCR was also used to study the SgrS expression level and to check for *pfkA* overexpression using the SYBR Green-based detection protocol (Life Technology), an ICycler real-time PCR detection system (Biorad) and "MyIQ" software (Biorad), as described in Enjalbert *et al.* (2013).

Glycogen staining assays and intracellular glycogen quantification

Strains were grown overnight at 37°C in 50 ml M9 media containing either 2.7 g · l^{-1} *D*-glucose, 2.7 g · l^{-1} *D*-fructose, 2.45 g · l^{-1} *L*-fucose or 2.5 g · l^{-1} N-acetyl-(*D*)-glucosamine. The intracellular glycogen content of both *csrA51* and the wild-type strains was quantified at midexponential growth. The experiments were performed in biological and technical duplicate. The quantification was done as described in Parrou and François (1997). Briefly, the cells were lysed to extract the glycogen which was then hydrolysed by amyloglucosidase into glucose subunits. The glucose subunits were then quantified using a glucose oxidase coupled to the colorimetric reagent o-dianisidine dihydrochloride.

Metabolic flux analysis

A slightly modified version of the genome-scale reconstruction iAF1260-flux2 of *E. coli* was used for all simulations (Feist *et al.*, 2007). These were performed using the COBRAv2 Toolbox with Gurobi 6.0.4 as linear programming solver (Schellenberger *et al.*, 2011). The model and the definition of its maintenance fluxes and constraints are described in supporting information S2 and S3. In order to determine the intracellular distribution of fluxes consistent with the measured exchange fluxes and growth rate, we performed a metabolic flux analysis, where the objective was to minimize the measured and predicted exchange fluxes and growth rate. Let v denotes the vector of steady-state fluxes with lower bounds v^l and upper bounds v^u, N the stoichiometric matrix, u^+ and u^- non-negative dummy fluxes, and u^M the vector of p measurements of exchange fluxes and growth rate. We assume that the first p elements of v correspond to the measured fluxes. Similarly to what was done in Lee *et al.* (2012), the metabolic flux analysis can be then formulated as the following linear programming problem:

$$\min \sum_{j=1}^{p}(u_j^+ + u_j^-) \text{ subject to:}$$

$$Nv = 0,$$

$$v^l \leq v \leq v^u,$$

$$v_j - u_j^+ + u_j^- = u_j^M, \text{ for all } j = 1, \ldots, p,$$

$$u^+, u^- \geq 0.$$

Using this objective function, metabolic flux analysis was performed for the wild-type and *csrA51* strains, followed by a flux variability analysis (Mahadevan and Schilling, 2003) to analyse the space of solutions. This allowed us to obtain lower and upper bounds for reaction fluxes in the two strains that are consistent with the measured growth rate and exchange fluxes.

Hierarchical regulation analysis

Regulation analysis dissects flux regulation into a hierarchical regulation coefficient ρ_h and a metabolic coefficient ρ_m (van Eunen *et al.*, 2011). In this study, ρ_h quantifies to which extent changes of protein levels in the *csrA51* strain, resulting in the modification of enzyme-specific activities (SA), contribute to the change of flux (v):

$$\rho_h = \frac{\ln SA_{csrA} - \ln SA_{WT}}{\ln v_{csrA} - \ln v_{WT}}. \quad (7)$$

The coefficient ρ_m quantifies the effect of changes in the interaction of the enzyme with the rest of metabolism on the change of flux, through variations in the concentration of substrates, products and allosteric effectors. The coefficient ρ_h is directly determined from the data and the fluxes using Eq. (1), while the coefficient ρ_m is derived from the following summation theorem:

$$\rho_h + \rho_m = 1. \quad (8)$$

The regulation coefficients for each reaction were calculated from Eqs. (1) and (2) and combinations of the different replicates of enzyme-specific activities and the minimal and maximal flux values returned by the metabolic flux analysis (see supporting information S4 for details). The statistical distribution of the regulation coefficients for each reaction was represented by means of box plots. Wilcoxon signed-rank tests enabled us to statistically assess the type of regulation exerted by the metabolism and gene expression (see supporting information S4 for details).

Acknowledgments

We thank Alessandra Fontana, Andrea Belluati and Sophie Mondeil for their worthy contribution to this work and Hidde de Jong and Eugenio Cinquemani for fruitful discussions. This work was supported by the Institut National de la Recherche Agronomique (Department 'Microbiology of the Food Chain') and the Institut National de Recherche en Informatique et en Automatique) from which MM received a doctoral fellowship. It was also partially supported by the Agence Nationale de la Recherche under project RESET (ANR-11-BINF-0005). MetaToul (Metabolomics & Fluxomics Facitilies, Toulouse, France, www.metatoul.fr) and its staff members (Lara Gales and Lindsey Peyriga) are gratefully acknowledged for access to NMR or mass spectrometry facilities. MetaToul is part of the national infrastructure MetaboHUB-ANR-11-INBS-0010 (The French National infrastructure for metabolomics and fluxomics, www.metabohub.fr). Gene expression data were obtained with the support of the Genomic and Transcriptomic Platform of Auzeville.

References

Adams, J.L., and McLean, R.J. (1999) Impact of rpoS deletion on *Escherichia coli* biofilms. *Appl Environ Microbiol* **65**: 4285–4287.

Altier, C., Suyemoto, M., and Lawhon, S.D. (2000) Regulation of *Salmonella enterica* serovar typhimurium invasion genes by csrA. *Infect Immun* **68**: 6790–6797.

Antoniewicz, M.R. (2015) Methods and advances in metabolic flux analysis: a mini-review. *J Ind Microbiol Biotechnol* **42**: 317–325.

Bradford, M.M. (1976) A rapid and sensitive method for the quantitation of microgram quantities of protein utilizing the principle of protein-dye binding. *Anal Biochem* **72**: 248–254.

Castano-Cerezo, S., Pastor, J.M., Renilla, S., Bernal, V., Iborra, J.L., and Canovas, M. (2009) An insight into the role of phosphotransacetylase (pta) and the acetate/acetyl-CoA node in *Escherichia coli*. *Microb Cell Fact* **8**: 54. doi:10.1186/1475-2859-8-54.

Duss, O., Michel, E., Diarra, N., Schubert, M., and Allain, F. (2014) Molecular basis for the wide range of affinity found in Csr/Rsm protein–RNA recognition. *Nucleic Acids Res* **42**: 5332–5346.

Edwards, A.N., Patterson-Fortin, L.M., Vakulskas, C.A., Mercante, J.W., Potrykus, K., Vinella, D., *et al*. (2011) Circuitry linking the Csr and stringent response global regulatory systems. *Mol Microbiol* **80**: 1561–1580.

Enjalbert, B., Jourdan, F., and Portais, J.C. (2011) Intuitive visualization and analysis of multi-omics data and application to *Escherichia coli* carbon metabolism. *PloS ONE* **6**: e21318.

Enjalbert, B., Letisse, F., and Portais, J.C. (2013) Physiological and molecular timing of the glucose to acetate transition in *Escherichia coli*. *Metabolites* **3**: 820–837.

Esquerre, T., Laguerre, S., Turlan, C., Carpousis, A.J., Girbal, L., and Cocaign-Bousquet, M. (2014) Dual role of transcription and transcript stability in the regulation of gene expression in *Escherichia coli* cells cultured on glucose at different growth rates. *Nucleic Acids Res* **42**: 2460–2472.

van Eunen, K., Rossell, S., Bouwman, J., Westerhoff, H.V., and Bakker, B.M. (2011) Quantitative analysis of flux regulation through hierarchical regulation analysis. *Methods Enzymol* **500**: 571–595.

Even, S., Lindley, N.D., and Cocaign-Bousquet, M. (2001) Molecular physiology of sugar catabolism in Lactococcus lactis IL1403. *J Bacteriol* **183**: 3817–3824.

Feist, A.M., Henry, C.S., Reed, J.L., Krummenacker, M., Joyce, A.R., Karp, P.D., *et al*. (2007) A genome-scale metabolic reconstruction for *Escherichia coli* K-12 MG1655 that accounts for 1260 ORFs and thermodynamic information. *Mol Syst Biol* **3**: 121. Epub 2007 Jun 26.

Fischer, E., and Sauer, U. (2003) Metabolic flux profiling of *Escherichia coli* mutants in central carbon metabolism using GC-MS. *Eur J Biochem* **270**: 880–891.

Heinemann, M., and Sauer, U. (2010) Systems biology of microbial metabolism. *Curr Opin Microbiol* **13**: 337–343.

Holms, H. (1996) Flux analysis and control of the central metabolic pathways in *Escherichia coli*. *FEMS Microbiol Rev* **19**: 85–116.

Joshi, J.G. (1982) Phosphoglucomutase from Yeast. *Methods Enzymol* **89**: 599–605.

Kotte, O., Zaugg, J.B., and Heinemann, M. (2010) Bacterial adaptation through distributed sensing of metabolic fluxes. *Mol Syst Biol* **6**: 355. doi:10.15252/msb.20135022.

ter Kuile, B.H., and Westerhoff, H.V. (2001) Transcriptome meets metabolome: hierarchical and metabolic regulation of the glycolytic pathway. *FEBS Lett* **500**: 169–171.

Lee, D., Smallbone, K., Dunn, W.B., Murabito, E., Winder, C.L., Kell, D.B., *et al*. (2012) Improving metabolic flux predictions using absolute gene expression data. *BMC Syst Biol*. **6**: 73. doi:10.1186/1752-0509-6-73.

Liu, M.Y., Yang, H., and T. Romeo (1995) The product of the pleiotropic *Escherichia coli* gene *csrA* modulates glycogen biosynthesis via effects on mRNA stability. *J Bacteriol* **177**: 2663–2672.

Mahadevan, R., and Schilling, C.H. (2003) The effects of alternate optimal solutions in constraint-based genome-scale metabolic models. *Metab Eng* **5**: 264–276.

Mao, F., Leung, W.Y., and Xin, X. (2007) Characterization of EvaGreen and the implication of its physicochemical properties for qPCR applications. *BMC Biotechnol* **7**: 76. doi:10.1186/1472-6750-7-76.

McKee, A.E., Rutherford, B.J., Chivian, D.C., Baidoo, E.K., Juminaga, D., Kuo, D., *et al*. (2012) Manipulation of the carbon storage regulator system for metabolite remodeling and biofuel production in *Escherichia coli*. *Microb Cell Fact* **11**: 79. doi:10.1186/1475-2859-11-79.

Morita, T., El-Kazzaz, W., Tanaka, Y., Inada, T., and Aiba, H. (2003) Accumulation of glucose 6-phosphate or fructose 6-phosphate is responsible for destabilization of glucose transporter mRNA in *Escherichia coli*. *J Biol Chem* 15608–15614.

Nakahigashi, K., Toya, Y., Ishii, N., Soga, T., Hasegawa, M., Watanabe, H., *et al*. (2009) Systematic phenome analysis of *Escherichia coli* multiple-knockout mutants reveals hidden reactions in central carbon metabolism. *Mol Syst Biol* **5**: 306. doi:10.1038/msb.2009.65.

Nguyen, D., Joshi-Datar, A., Lepine, F., Bauerle, E., Olakanmi, O., Beer, K., *et al*. (2011) Active starvation responses mediate antibiotic tolerance in biofilms and nutrient-limited bacteria. *Science* **334**: 982–986.

Parrou, J.L., and François, J. (1997) A simplified procedure for a rapid and reliable assay of both glycogen and trehalose in whole yeast cells. *Anal Biochem* **248**: 186–188.

Peng, L., and Shimizu, K. (2003) Global metabolic regulation analysis for *Escherichia coli* K12 based on protein expression by 2-dimensional electrophoresis and enzyme activity measurement. *Appl Microbiol Biotechnol* **61**: 163–178.

Revelles, O., Millard, P., Nougayrede, J.P., Dobrindt, U., Oswald, E., Letisse, F., and Portais, J.C. (2013) The carbon storage regulator (CSR) system exerts a nutrient-specific control over central metabolism in *Escherichia coli* strain Nissle 1917. *PloS ONE* **8**: e66386.

Rice, J.B., and Vanderpool, C.K. (2011) The small RNA SgrS controls sugar-phosphate accumulation by regulating multiple PTS genes. *Nucleic Acids Res* **39**: 3806–3819.

Romeo, T., Gong, M., Liu, M.Y., and Brunzinkernagel, A.M. (1993) Identification and molecular characterization of *csrA*, a pleiotropic gene from *Escherichia coli* that affects

glycogen biosynthesis, gluconeogenesis, cell size, and surface properties. *J Bacteriol* **175**: 4744–4755.
Romeo, T., Vakulskas, C.A., and Babitzke, P. (2013) Post-transcriptional regulation on a global scale: form and function of Csr/Rsm systems. *Environ Microbiol* **15**: 313–324.
Sabnis, N.A., Yang, H., and Romeo, T. (1995) Pleiotropic regulation of central carbohydrate metabolism in *Escherichia coli* via the gene *csrA*. *J Biol Chem* **270**: 29096–29104.
Sabourin, D., and Beckwith, J. (1975) Deletion of the *Escherichia coli* crp gene. *J Bacteriol* **122**: 338–340.
Sauer, U., Lasko, D.R., Fiaux, J., Hochuli, M., Glaser, R., Szyperski, T., *et al*. (1999) Metabolic flux ratio analysis of genetic and environmental modulations of *Escherichia coli* central carbon metabolism. *J Bacteriol* **181**: 6679–6688.
Schellenberger, J., Que, R., Fleming, R.M., Thiele, I., Orth, J.D., Feist, A.M., *et al*. (2011) Quantitative prediction of cellular metabolism with constraint-based models: the COBRA Toolbox v2.0. *Nat Protoc* **6**: 1290–1307.
Seyll, E., and Van Melderen, L. (2013) The ribonucleoprotein Csr network. *Int J Mol Sci* **14**: 22117–22131.
Shimizu, K. (2014) Regulation systems of bacteria such as *Escherichia coli* in response to nutrient limitation and environmental stresses. *Metabolites* **4**: 1–35.
Smallbone, K., Messiha, H.L., Carroll, K.M., Winder, C.L., Malys, N., Dunn, W.B., *et al*. (2013) A model of yeast glycolysis based on a consistent kinetic characterisation of all its enzymes. *FEBS Lett* **587**: 2832–2841.
Taymaz-Nikerel, H., de Mey, M., Ras, C., ten Pierick, A., Seifar, R.M., van Dam, J.C., *et al*. (2009) Development and application of a differential method for reliable metabolome analysis in *Escherichia coli*. *Anal Biochem* **386**: 9–19.
Timmermans, J., and Van Melderen, L. (2009) Conditional essentiality of the *csrA* gene in *Escherichia coli*. *J Bacteriol* **191**: 1722–1724.
Timmermans, J., and Van Melderen, L. (2010) Post-transcriptional global regulation by CsrA in bacteria. *Cell Mol Life Sci* **67**: 2897–2908.
Vanderpool, C.K. (2007) Physiological consequences of small RNA-mediated regulation of glucose-phosphate stress. *Curr Opin Microbiol* **10**: 146–151.
Van der Werf, M.J., Guettler, M.V., Jain, M.K., and Zeikus, J.G. (1997) Environmental and physiological factors affecting the succinate product ratio during carbohydrate fermentation by Actinobacillus sp. 130Z. *Arch Microbiol* **167**: 332–342.
Wei, B., Shin, S., LaPorte, D., Wolfe, A.J., and Romeo, T. (2000) Global regulatory mutations in *csrA* and *rpoS* cause severe central carbon stress in *Escherichia coli* in the presence of acetate. *J Bacteriol* **182**: 1632–1640.
Wei, Y., Lee, J.M., Smulski, D.R., and LaRossa, R.A. (2001) Global impact of *sdiA* amplification revealed by comprehensive gene expression profiling of *Escherichia coli*. *J Bacteriol* **183**: 2265–2272.
Yakhnin, A.V., Baker, C.S., Vakulskas, C.A., Yakhnin, H., Berezin, I., Romeo, T., and Babitzke, P. (2013) CsrA activates flhDC expression by protecting *flhDC* mRNA from RNase E-mediated cleavage. *Mol Microbiol* **87**: 851–866.
Yang, H., Liu, M.Y., and Romeo, T. (1996) Coordinate genetic regulation of glycogen catabolism and biosynthesis in *Escherichia coli* via the *csrA* gene product. *J Bacteriol* **178**: 1012–1017.